REGIONAL NOWCASTING OF THE SOLAR POWER PRODUCTION WITH PV-PLANT MEASUREMENTS AND SATELLITE IMAGES

Yves-Marie Saint-Drenan[1*], Stefan Bofinger[1], Bernhard Ernst[2], Thomas Landgraf[3] and Kurt Rohrig[1]

[1] Fraunhofer Institute for Wind Energy and Energy System Technology, Kassel (Germany)

[2] SMA Solar Technology AG, Niestetal (Germany)

[3] Enercast GmbH, Kassel (Germany)

* Corresponding Author, y.saint-drenan@iwes.fraunhofer.de

1. Introduction

With a rapid development of the installed PV-capacity during the last years, the influence of the PV-power generation on the power system increased. Since only ca. 25% of the PV-plants are monitored, the German system operators need to implement system to monitor the current PV-power production in their region (nowcasting system). In this paper, a method based on the combined use of satellite data and measurement is proposed to improve the accuracy of the assessment of regional PV-power production.

2. Need for a PV-nowcasting system for the integration of the PV-energy

For the last years the installed PV-capacity has been rapidly increasing so that it currently represents a significant share of the energy mix. The development of the installed PV-capacity has been especially important in 2010. During this year ca. 7 GW_p were installed, bring about an increase of 70% of the installed capacity (see Fig.1).

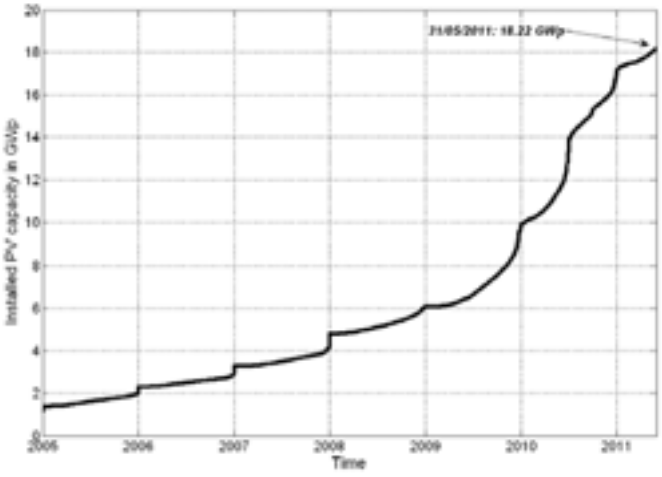

Fig. 1: Development of the installed PV capacity in Germany

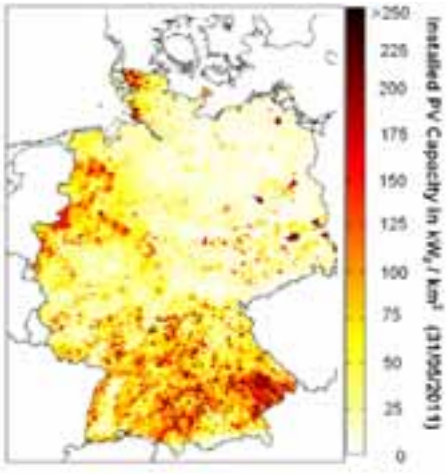

Fig. 2: Geographical distribution of the installed capacity at the end of May 2011

Before this year, the influence of the PV power on the power system was often underestimated by many DSOs. At this time, the German DSOs and energy utilities were responsible for the prediction and the nowcasting of the PV-power. A large share of PV-power generation was integrated as base load or as weather-independent standard profiles. Only large PV-plants were equipped with a 15-minute metering system and balanced online. Furthermore, exact information on the current status of the installed capacity was not available but yearly updated. As a result, appropriate mechanisms for the integration of the PV-power production were not available as the strong deployment of the installed PV capacity occurred.

In September 2010, this situation conducted to noticeable effects on the power system. On September the 6th a positive imbalance of 7 GW occurred for several hours due to an unexpected overproduction of PV-power. The complete negative balancing reserve power (4 300 MW) as well as additional balancing power from neighboring countries (ca. 2 800 MW) was used to balance this excess, which conducted to important costs. A detailed description on this event can be found in Thomaschki (2011). The time series of the PV-power production and the balancing energy for September 2010 are given in Fig.3.

During the other days of September 2010, the influence of the PV generation on the needed balancing power is clearly recognizable whereas not as extreme as on September, the 6th. The influence of the PV-power generation on the balance power is illustrated in Fig.4.

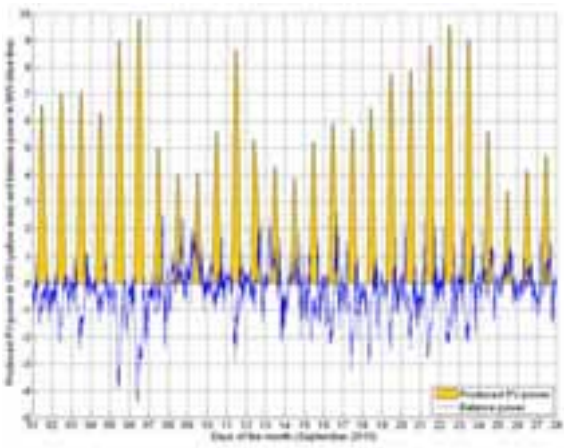

Fig. 3: PV power production and balancing energy in September 2011

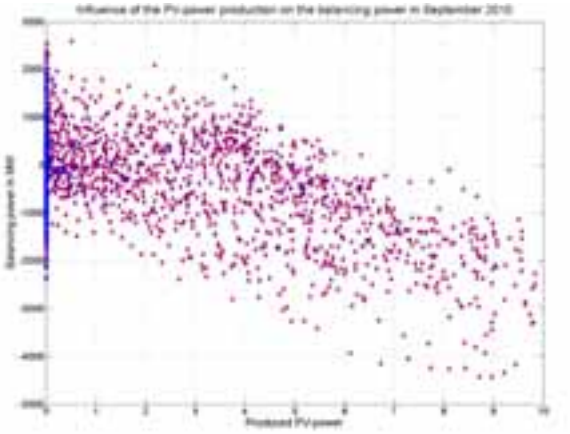

Fig.4: Scatter plot of the balance energy as a function of the PV power production

The event of 2010, September the 6th raised the need for appropriate mechanisms for the integration of the PV-power in the energy system. In particular, the German regulator (Bundesnetzagentur) made recommendations aiming at improving the PV-nowcasting systems implemented by the 823 German DSOs (Thomaschki, 2011). Due to the fact that approximately 75% of the ca. 900 000 German PV plants are not measured, an algorithm has to be implemented to assess the current PV-production in a region based on an upscaling algorithm taking into account the characteristics of the installed PV-capacity and meteorological factors (Nowcasting system).

The 823 German network operators are displayed in the map in Fig.5. The area of the region covered by the DSOs is represented as a probability density distribution in Fig.6. It can be observed in Fig.6 that the area covered by the majority of the DSO is very small: 613 of the 823 DSOs cover an area smaller than 100 km^2. Therefore, the nowcasting system needs to have a good accuracy on length scales smaller than 10 km (root of 100 km^2). In addition, since the PV-power generation is traded into the energy market (EEG 2009), the PV-power generation needs to be assessed by the nowcasting system on a 15-minute basis.

One of the questions addressed in this paper is to find out if the accuracy of current nowcasting systems is sufficient on the time and length scale identified and to propose a methodology adapted to the current needs.

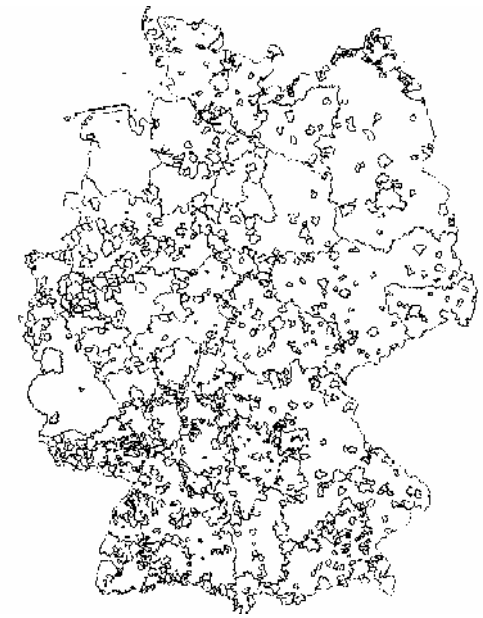

Fig. 5: Map of Germany with the control zone of the 823 German DSOs

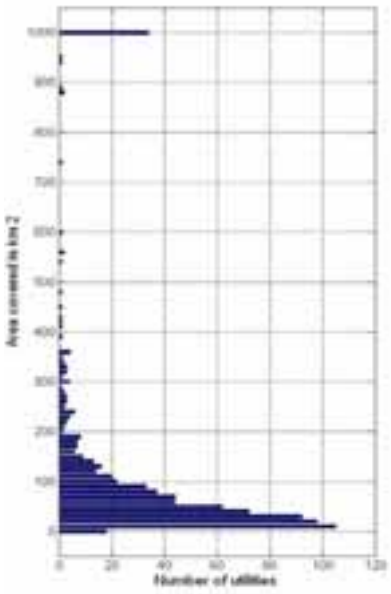

Fig. 6: Probability density distribution of the surface covered by the DSO control zones

3. State of the art of existing PV-nowcasting systems

The four German TSOs have been using nowcasting and forecasting systems for PV-power for several years. The method used in these systems conducts to satisfying results for the large region covered by the TSOs. The principle consists in an interpolation of the normalized power of a set of reference PV-plants on a raster covering the area considered. The interpolated values are then multiplied with the installed capacity for each cell of the raster. The interpolation technique used is generally the Shepherd's method which given in (eq. 1) and (eq.2) and illustrated in Fig. 7.

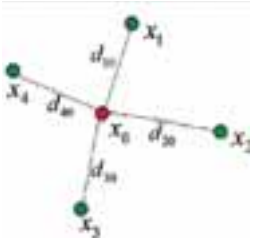

$$u(x) = \sum_{i=1}^{N} w_i(x) \cdot u(x_i) \qquad \text{(eq. 1)}$$

$$w_i(x) = \frac{d(x, x_i)^{-p}}{\sum_{k=1}^{N} d(x, x_k)^{-p}} \qquad \text{(eq. 2)}$$

Fig. 7: Principle and equation of the inverse distance weighting (IDW) interpolation method

The idea of this interpolation method is to evaluate the missing value $d(x_0)$ for the point x_0 as the weighted sum of values $d(x_i)$ at the neighboring points x_i. The closer the point x_0 is, the larger the weight w_i for the value $d(x_i)$ is. As example the method used by the German TSO EnbW can be found in (Schierenbeck et al, 2010) or (Rohrig et al 2003).

To evaluate the performance of this method, the measurements of the SMA database (Sunny Portal, ca. 5000 PV-plants used for this study) were used. The locations of the PV-plants are displayed in Fig.8. For each PV-plant, the normalized power is represented by the color of the point (2011, August the 15th at 12:00). The map of irradiation derived from a satellite image for this time is given in Fig.9.

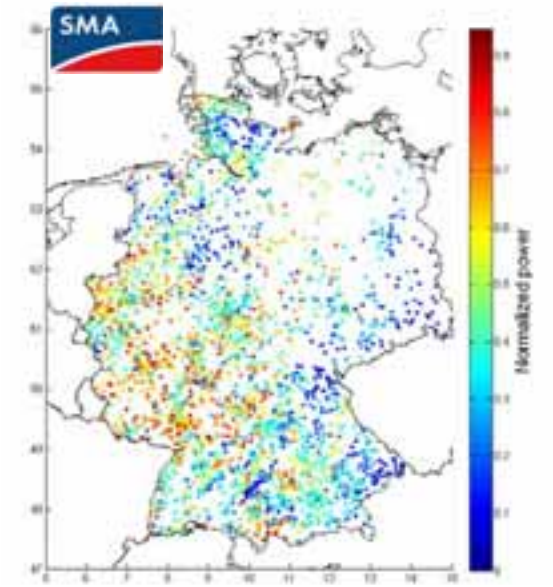

Fig. 8: PV plant of the Sunny Portal (SMA) – the color of the points represents the normalized power on 15/08/2011 at 12:00

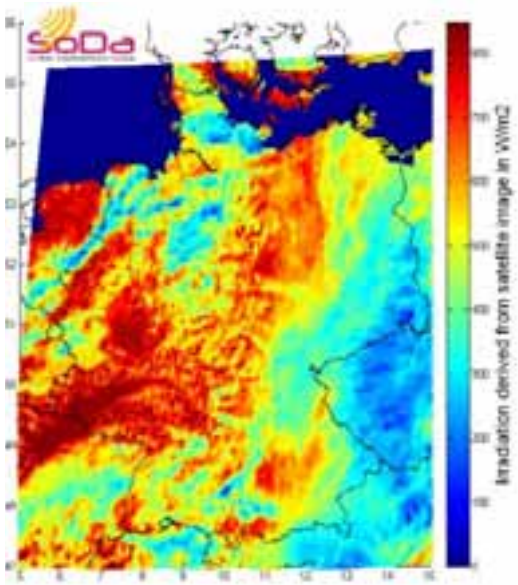

Fig. 9: Irradiation derived from satellite picture on 15/08/2011 at 12:00 (www.soda-is.com)

Assuming at this step, that the satellite image is a good approximation of the actual irradiation over Germany, it can be observed that the general pattern of the cloud structures can be recognized with the SMA data. Furthermore, a comparison of the SMA map of Fig. 8 with the map of the installed capacity in Fig.2 shows that the geographical distribution of the SMA data is related to the distribution of the installed capacity. This means that on the one hand where the installed capacity is large, the probability that a measurement is available is high. On the other hand, the interpolation error will be large were the installed capacity is small.

Therefore, it can be reasonably expected that the result of the above described method conducts to an improvable but satisfying accuracy for the large region covered by the TSOs. On the smaller length scale of the DSO regions, this argumentation is not valid any more and the accuracy of this simple interpolation method for the DSO needs to be evaluated.

To address this issue, a 7x7km raster covering Germany was used. For each cell of this raster, the distance to the next available measurement was evaluated. The results are displayed in Fig. 11 as a map and in Fig. 9 as a probability density distribution (red histogram, y-axis on the right side). It can be seen that the majority of the cells is not further that 30 km to the next PV-plant. 40 % of the cells have a PV-plant in less than 5 km, 75% in less than 10 km and 96% in less than 20 km.

In order to evaluate the influence of the distance to the next measurement on the interpolation error, the correlation between each possible combination of two PV-plants has been evaluated. Only data between 9 and 15 hour (solar time) were used. The average correlation between two measurements is represented as a function of the distance in Fig. 10 (blue line, y-axis on the left side). In addition, the correlation was also evaluated for the global horizontal irradiation at each measurement points using data derived from satellite pictures (green line in Fig. 10, y-axis on the left side).

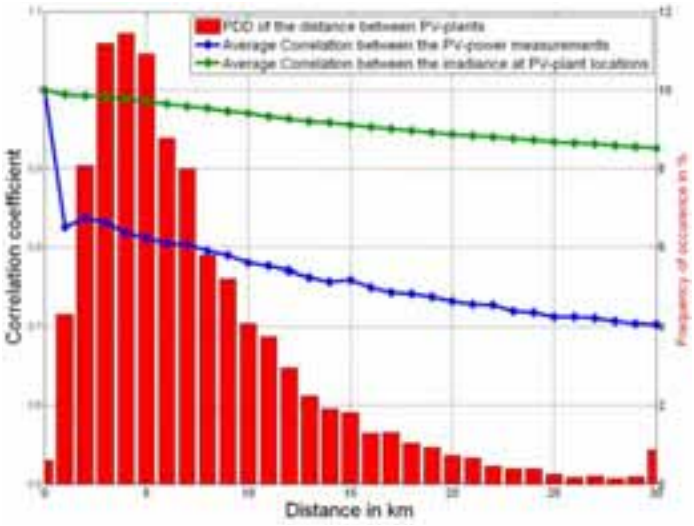

Fig. 10: Dependence of the average correlation between PV-power and irradiation at two locations as a function of the distance separating them (blue and green curves) and PDD of the distance between each cell of a 7x7 km raster and the next SMA PV-plant

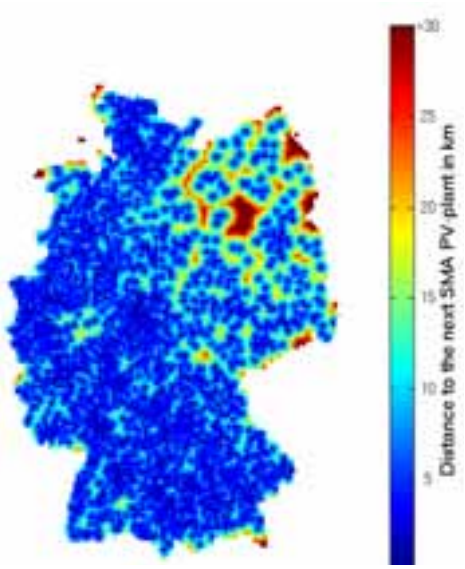

Fig. 11: Distance between each cell of a 7x7 km raster and the next SMA PV-plant

The high correlation values between the irradiance at two locations (green line on the left graphic of Fig. 10) are due to the influence of the sun position on the irradiance (similar daily and yearly profile due to the earth rotation and earth declination respectively). A correction for the influence of the solar geometry such as the one proposed in (Perez 2011) would significantly decrease these values. It was decided not to apply this correction, since it is difficult to apply to power measurements.

A comparison of the blue and green lines of Fig.10 shows that for any distance the correlation between the irradiation is higher than the correlation between PV-power measurements. This difference is much larger than the influence of the distance. Investigation on the source of this discrepancy showed, that the characteristics of the PV plants (especially the module orientation) are responsible for the observed reduction of the correlation (see Fig. 12 and 13).

The small decrease of the correlation with the distance is due to the fact that the influence of the solar position was not corrected. However, this should be relativized: a look at Fig.8 shows that, for a given time step, in regions were the regional gradient of the irradiation is large; the relative uncertainty can exceed 50% for a given point. For large DSO, this error will be reduced with the smoothing effects but this is not the case for the majority of the German DSOs.

For most location in Germany, the nowcasting methods based on the interpolation PV-plant measurements are based on measurement data, whose correlation is smaller than 0.8. A further investigation using Kriging error assessment method would allow a first quantification of the error but it is already clear that the accuracy will not meet the need of most of the German DSOs.

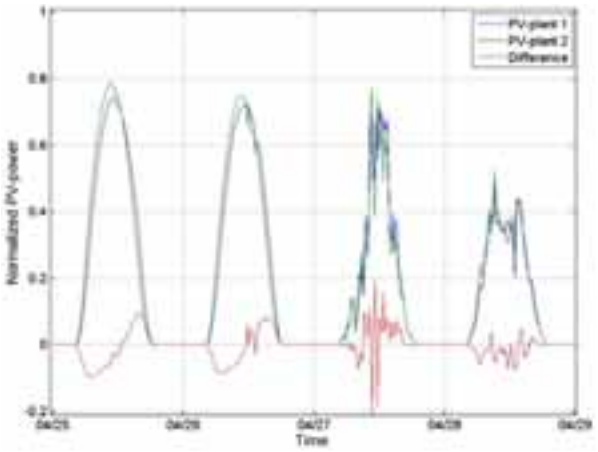

Fig. 12: PV-Power of two PV plants located in the same zip area (PLZ=25709, surface=69km²)

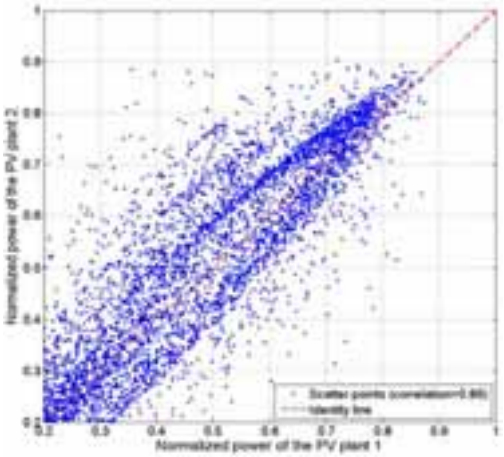

Fig. 13: Scatter plot of two PV plants located in the same zip area (PLZ=25709, surface=69km²)

4. Principle and accuracy of satellite-based radiation assessment methods

The regional distribution of the PV plants and the influence of the PV plants characteristics have a strong influence on the accuracy of the regional nowcasting methods. The use of satellite image to assess the irradiation has become a proven technique and been widely used over the last years. Satellite information would allow getting information on the weather situation where PV-power measurements are lacking. Furthermore, it would offer the chance to take into account the characteristics of the PV-plant used and thus potentially reduce the uncertainty described in the last section.

4.1. Derivation of the ground short wave radiation from satellite images

The images used for the assessment of the irradiation are coming from the image of the visible channels of the geostationary satellite meteosat-9. In order to assess the ground irradiation from the satellite image, a relation is used between these two values. Using the notation described in Fig. 14 a radiation budget at the ground gives the following equation:

$$G_{ground} = I_{sc} \cdot \varepsilon \cdot \cos(\theta_z) \cdot \left[\frac{T_{sc} T_c T_{cg}}{1 - A_S A_C T_{cg}^2} \right] \qquad \text{(eq. 3)}$$

where G_{ground} is the global horizontal irradiation at the ground for the pixel considered, I_{sc} is the solar constant and θ_z is the zenith angle. The meaning of the other parameters in eq. 3 is given in Fig.14.

The reflectance $A_{satellite}$ at the satellite can be derived using the zenith angle and the angle between the pixel and the satellite. A radiation budget at the satellite location gives the following relation:

$$A_{satellite} = A_R + T_{sc} A_C T_{cl-sat} + \frac{T_{sc} T_c^2 T_{cg} A_S T_{cl-sat}}{1 - A_c T_{cg}^2 A_s} \qquad \text{(eq. 4)}$$

Using different formulations of the transmission coefficients and albedo in eq.3 can 4 allows solving the equation system. There are differences between the approaches used by the different existing method for establishing the relationship between the ground irradiation and the satellite reflectance. For example the method developed by Meteo-France and implemented in LSA-SAF makes a physical formulation of the different terms in Eq.3 and 4 while the Helioclim-3 algorithm developed by Ecole des Mines de Paris based on an empirical relationship between the reflectance and the global horizontal irradiation. This relationship is motivated by the system of equation (eq.3 and 4). For the sake of conciseness, all details of these methods are not given here but can be found in the literature (SAF-DSSF, 2011) (Rigollier et al, 2004)

The common feature of all the algorithms is that information on the ground albedo and on the turbidity of the atmosphere needs to be known for the assessment of the ground irradiation. In addition, the irradiation values are based on the reflectance of the upper layer of the clouds. The diffusion and absorption processes occurring under this upper layer cannot be accurately assessed.

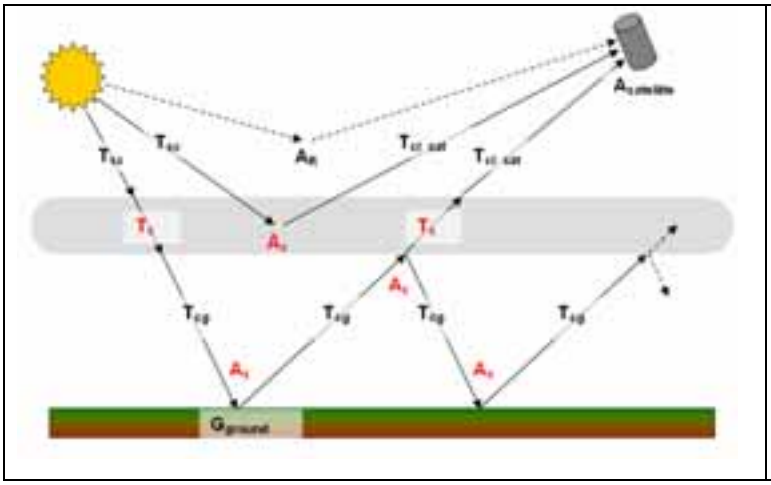

T_{sc}: transmittance of the atmosphere between the sun and the cloud

T_c: cloud transmittance

T_{cg}: transmittance of the atmosphere between the cloud and the ground

T_{cl_sat}: transmittance of the atmosphere between the cloud and the satellite

A_R: albedo due to Rayleigh scattering above the cloud

A_c: cloud albedo

A_s: surface albedo

Fig. 14: Parameters for the radiation budget at the ground and at the satellite needed for the derivation of the global horizontal irradiation form satellite images – adapted from (SAF-DSSR 2011)

In Fig.15 an exemplary day profile with direct, diffuse and satellite-derived irradiation is shown. The irradiation measurements from the BSRN measurement network for the Payern station (Switzerland) were used. It can be observed that the satellite values are fitting the global horizontal irradiation very well at the exception of a few fluctuations, which couldn't be assessed by the satellite. These fluctuations are mainly due to the presence of small clouds and to the reflection of the direct radiation on the clouds. In order to illustrate the principle of the satellite-based irradiation assessment, 8 time steps have been marked in Fig.15, for which satellite pictures from the channel 12 in the region of Payern are provided in Fig.16. It is important to note that the irradiation was not derived with these pictures but with pictures of a lower resolution. The satellite pictures were provided by the University of Oldenburg for this study.

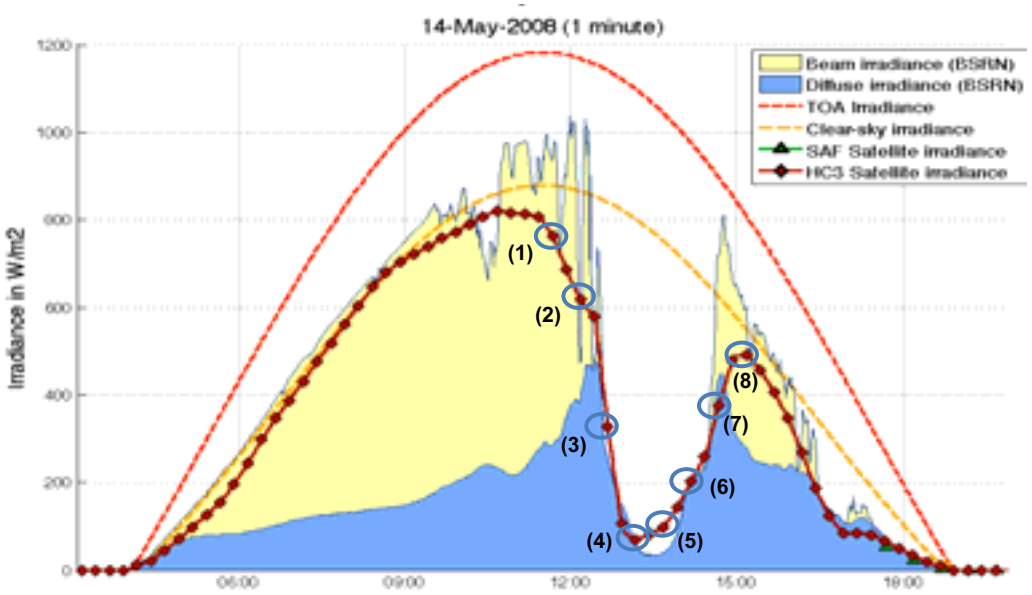

Fig. 15: Exemplary day with BSRN measurements and satellite-derived irradiation for the Payern station

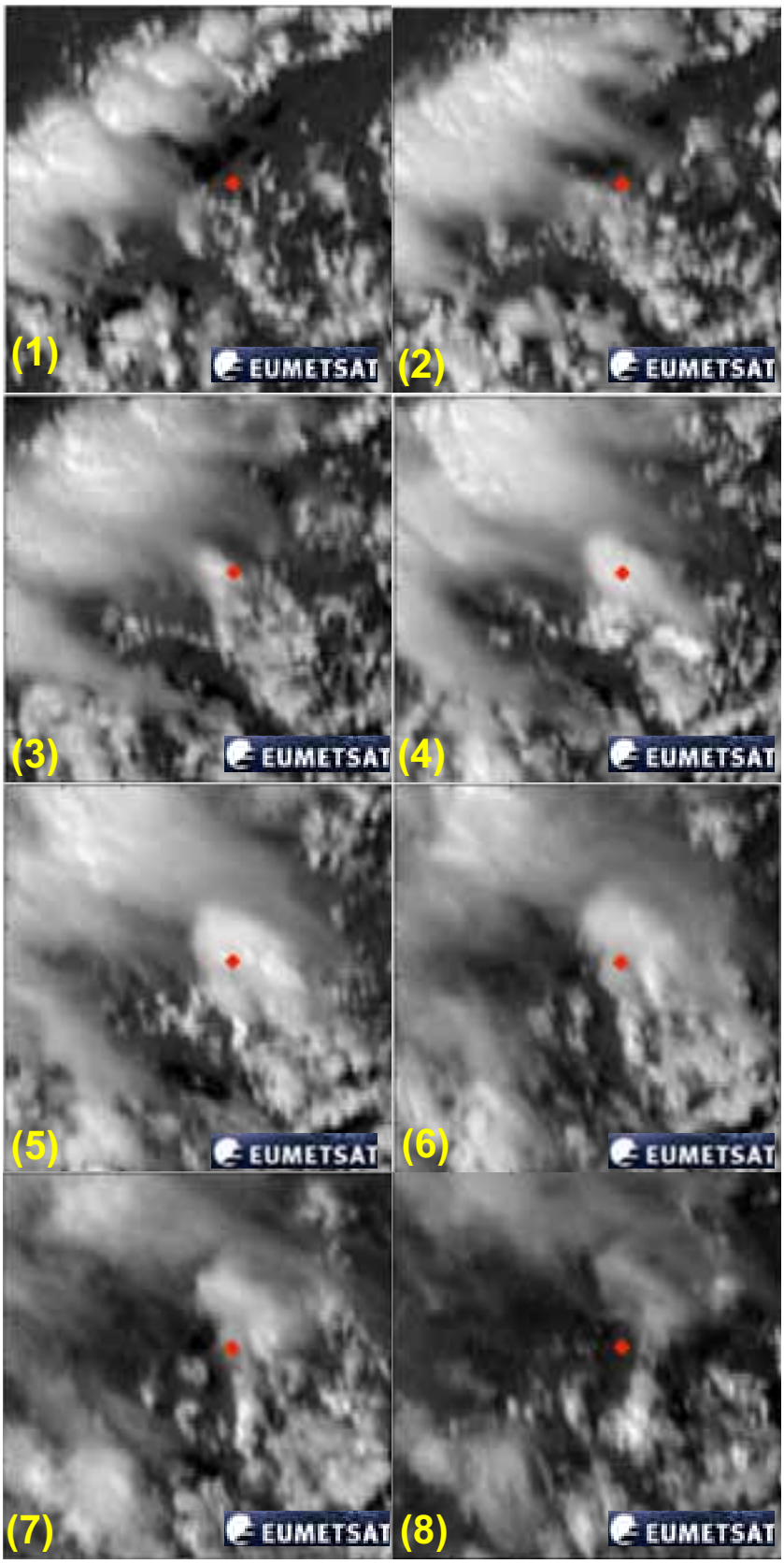

Fig. 16: Satellite images from the channel 12 of meteosat-9 in the region of Payern (station marked with a red diamond) for the time step marked in Fig.8 – The satellite picture were provided for this study by the University of Oldenburg

4.2. Assessment of the accuracy of the satellite image derived radiation

To integrate the satellite data to the PV-nowcasting system an important pre-requisite is to assess the accuracy of the satellite-derived irradiation and to understand the different mechanisms conducting to deviations between the estimated and the observed values. For this purpose the irradiation data from the SODA web platform (www.soda-is.com) and from the LSA-SAF service (landsaf.meteo.pt) were compared to the diffuse and direct irradiation measurements of the BSRN station of Payern. One-minute data and 15-minute average were used for this analysis. A detailed statistical analysis and visual check was carried out to get an insight on the performance of the satellite-derived irradiation. Different measures of the accuracy of the satellite data are given in table 1 for the 15-minute average of one year of measurements from the Payern station (2008).

Tab. 1: Statistical analysis of the error of the satellite-derived irradiation (Payern, 15-minute average of one year of data)

	LSA-SAF	HC3
Mean error	3.9 W/m2	11,3 W/m2
Mean absolute error	59.8 W/m2	48.7 W/m2
RMSE	105.6 W/m2	73.0 W/m2
Correlation	91,73	96.03
50% quantile of the absolute error	28 W/m2	33 W/m2
90 % quantile of the absolute error	148 W/m2	112 W/m2

In the comparison of satellite-based irradiation with measurements, it appeared that the error is very different for different classes of the diffuse fraction K_d (ratio of the diffuse irradiation to the global horizontal irradiation). This dependency is illustrated in Fig. 17 and 18.

The accuracy of the satellite date is the lowest for overcastted sky conditions (K_d>0.9). In this case the irradiation is derived from the upper cloud layer. The effect of diffusion and absorption processes on the ground irradiation produced by clouds eventually present under the upper cloud layer can't be taken into account. An exemplary day representative for such errors is shown in Fig. 19-c. In this example, it can be observed that the time series of satellite irradiation forms an upper limit for the measured irradiation, which would tend to confirm the assumption for the source of error.

For intermediate values of the diffuse fraction, the broken clouds which partly obscure the sun prevail (Skartveit et al, 1998). A frequent error is due to the fluctuation of the irradiation measurement, which can't be assessed by the satellite due to its limited spatial resolution (5x5 km in Germany). Small clouds in a clear sky or small holes in a cloud layer are not seen by the satellite. The resulting errors is given in Fig 19-a and Fig.19-b.

For clear-sky conditions, deviations between the actual and the predicted ground albedo and atmospheric turbidity result in a typical error pattern, which is illustrated in Fig.19-d. Such errors were observed for some winter days. However, the accuracy of the satellite derived irradiation for clear-sky conditions is very good.

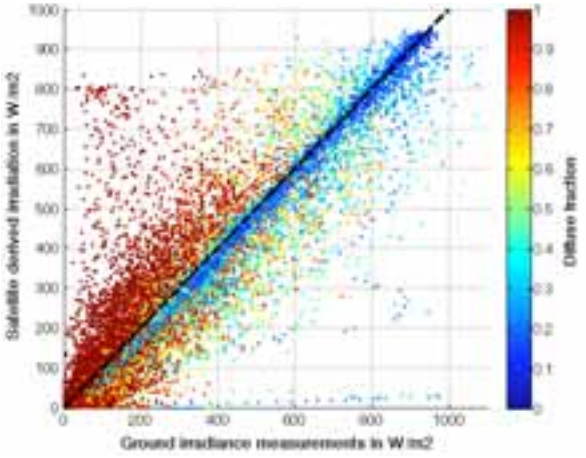

Fig. 17: Scatter plot of the LSA-SAF satellite derived irradiation as a function of the measured irradiation

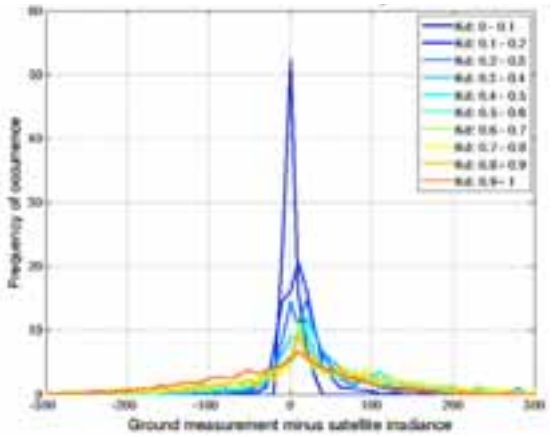

Fig. 18: Probability density distribution of the error of the LSA-SAF satellite derived irradiation for different classes of diffuse fraction

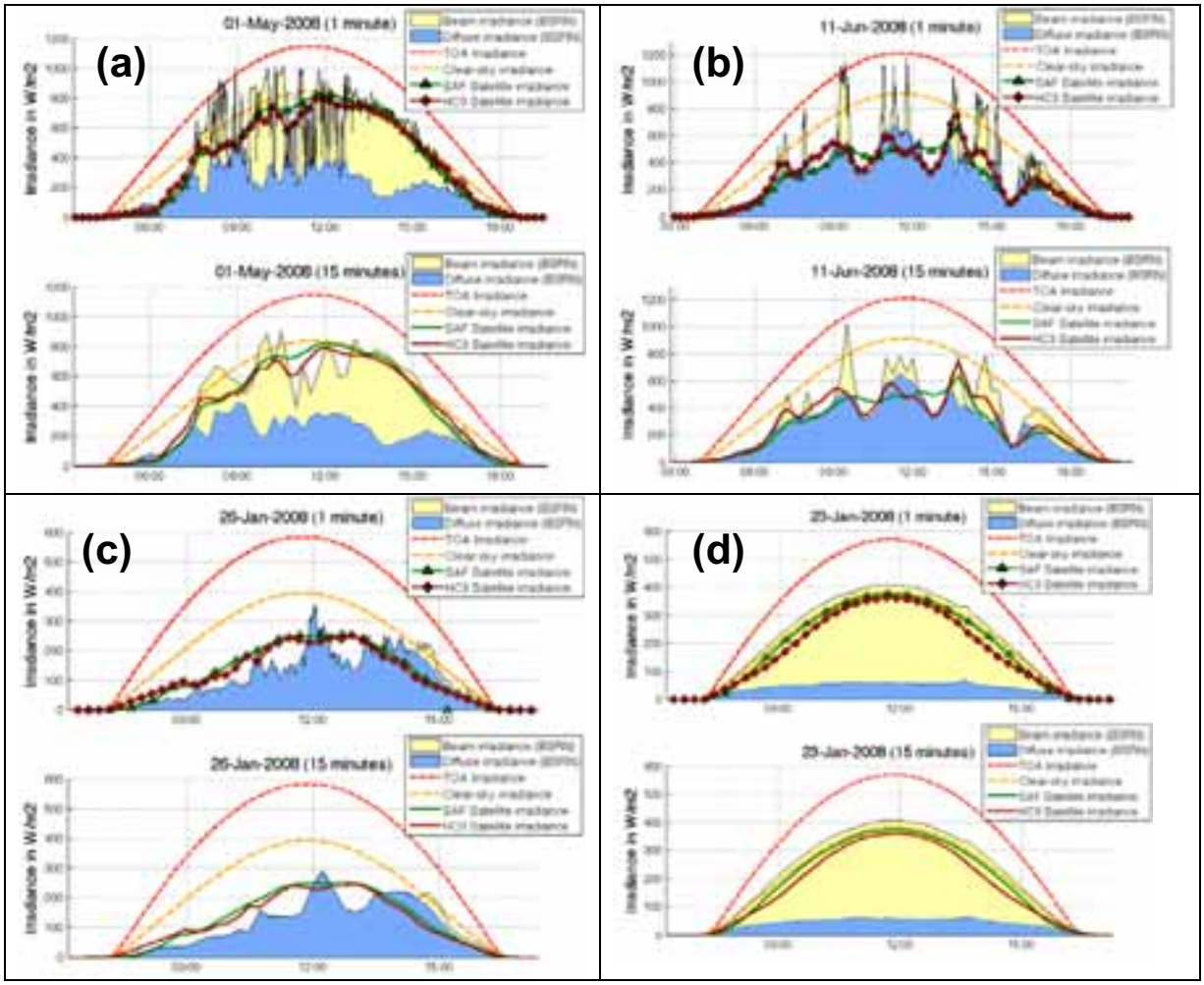

Fig. 19: Exemplary days showing the most frequent typical error patterns of satellite-derived irradiation

4.3. Correction of the satellite data using PV-power measurements

In order to improve the accuracy of the satellite-derived irradiation, a calibration of the irradiation was developed using measurement data from PV-plants.

In order to be able to compare PV-plant measurements with the satellite data, the global horizontal irradiation is derived from each PV-power measurement. This first step needs reliable information on the PV plants used and an exhaustive control of the different computation steps.

Using the irradiation derived from power data, calibration coefficients are calculated for each available location and interpolated to each cell of a raster covering Germany. The resulting correction coefficients are finally applied to the original satellite images.

Using this approach, the influence of phenomena conducting to errors for clear and overcastted sky conditions is reduced (ground albedo, atmospheric turbidity and effect of lower cloud layers). It can be expected that the interpolation of the local effects of small clouds on the ground irradiation may conduct to an error. However, it is assumed that the large number of PV-plants avoid this negative effect.

An additional benefit of this approach is that the influence of the PV-plant characteristics is separated from meteorological conditions. The problem illustrated in Fig 12 and 13 is thus addressed by the chosen method. In addition, PV-plant outages can be detected during the comparison of the PV-plant data with the satellite irradiation. The corresponding data can be filtered out and do not affect the quality of the interpolation.

Using this method the information contained in the satellite data and in the power measurement are merged, resulting to an improved assessment of the irradiation over Germany. The calculation of the PV-power from the global irradiation maps is described in the next section.

5. Integration of satellite radiation in a PV-nowcasting system

For the computation of the PV-power production for each DSO, a 7x7 km raster covering Germany is used. For each cell of this raster, the irradiation is obtained through the method described in the previous section. The air temperature is calculated with a Kriging interpolation of the free station measurements from the German weather service (DWD).

Using these meteorological data, a physical PV-plant model is used to simulate the PV-power. Each component of this model is based on state-of-the-art model validated using measurement from the Fraunhofer IWES.

The technological characteristics of the PV-plants were identified as very important factors for the accuracy of the nowcasting system. As a result, a very detailed analysis of several databases was carried out to determine the best set of parameters. It results from this analysis that the PV-plant characteristics are relatively homogeneous, when the PV-plants are classified according to their region, age and nominal power.

The nominal power of the PV-plant is the most important information for the classification. Indeed, the type of module, the type of montage, the characteristics of the inverter as well as the module orientation depends on this parameter. The influence of the nominal power on the tilt angle results from economical and architectural reasons. The larger the PV-plant, the higher is the probability that the orientation is optimal (30° South for Germany). For PV-plants which are not optimally orientated, the larger the PV-plant, the lower is the tilt angle. This may be explained by architectural and mechanical constraints. The consideration of the region is also very important: for example roofs with a tilt angle of 45° are very frequent in North Germany whereas in South Germany roofs with a tilt angle of 20-30° are very common.

The results of the model illustrated in Fig.12 are finally calibrated to the yearly production data of all PV-plants released yearly according to the EEG for each PV-plant class.

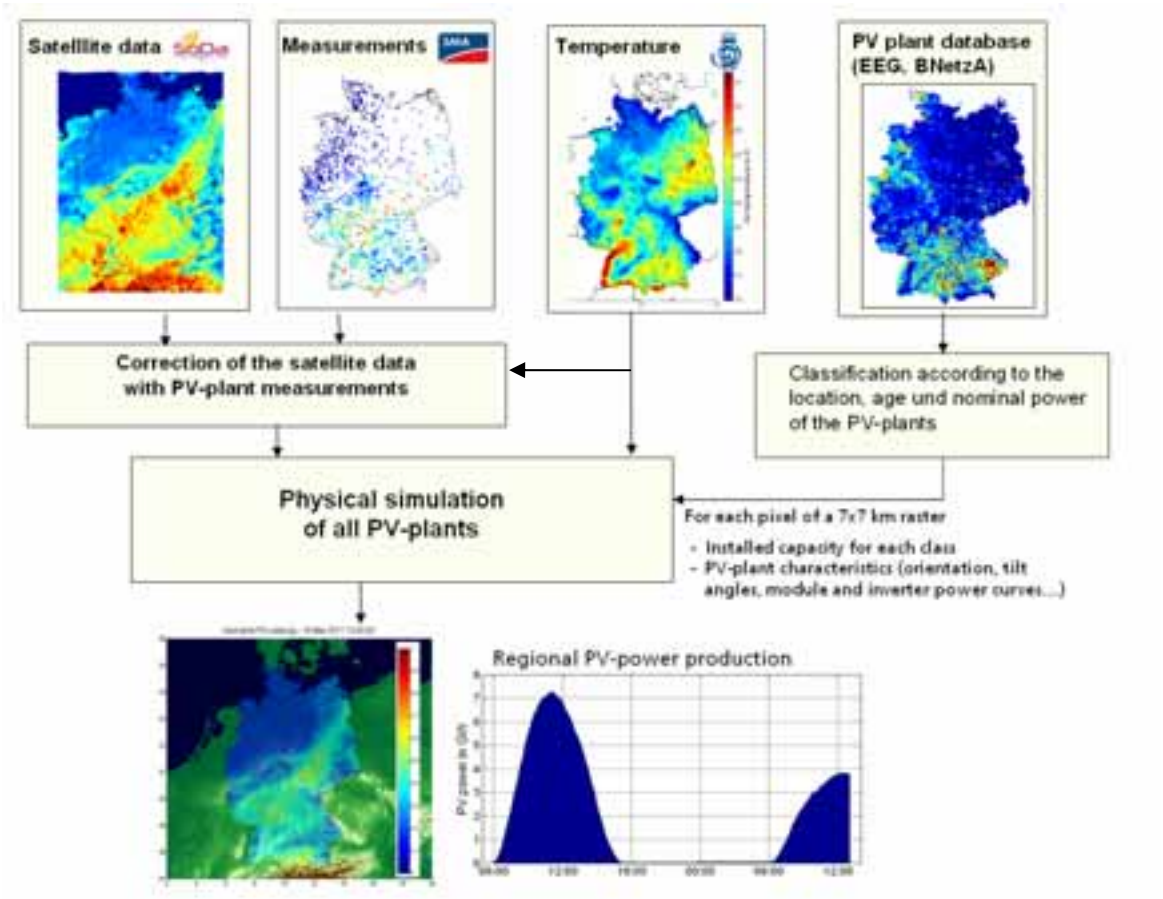

Fig. 12: Principle of the regional model developed at Fraunhofer IWES

6. Conclusion and outlook

The nowcasting system presented in this paper is aimed at improving the integration of the PV power into the power system. It has been developed for several years and appeared after the event of September 2010 to respond to an urgent need of the system operators.

It is currently being implemented by the company Enercast GmbH, which resulted from the activity of the Fraunhofer IWES in the field of RES prediction systems. Enercast GmbH is commercializing the presented system to the German system operators. It is currently implemented at several German TSOs and DSOs.

The development of the PV-nowcasting system is a first step in the development of a regional solar prediction system. The PV-model presented in Section 5 is currently being integrated in a PV-prediction system using different meteorological models (DWD, Meteo-France, ECMWF).

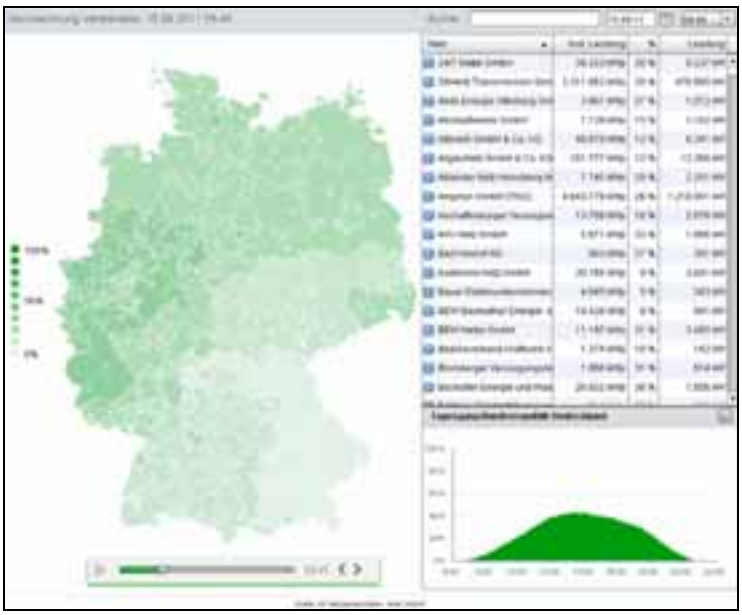

Fig. 13: Nowcasting system implemented on www.enercast.de

7. References

Gesetz für den Vorrang Erneuerbarer Energien (Erneuerbare-Energien-Gesetz – EEG), 25.10.2008

LSA-SAF, Product User Manual – Down-welling Surface Shortwave Flux (DSSF), EUMETSAT Satellite Application Facility on Land Surface Analysis, 2011

Perez, R., Kivalov. S., Schlemmer J., Hemker C., Hoff T., Short-term irradiance variability: Staion pair correlation as a function of distance, Submitted to Solar Energy, 2011

Rigollier C., Lefèvre M., Wald L., 2004, The method Heliosat-2 for deriving shortwave solar radiation data from satellite images. Solar Energy, 77(2), 159-169

Rohrig, K.; Ernst, B.; Hoppe-Kilpper, M.; Schlögl, F., 2003, Online-monitoring and prediction of wind power in german transmission system operation centres, WWEA, Bonn

Schierenbeck, S., Graeber, D. Semmig A., and Weber A., 2010, Ein distanzbasiertes Hochrechnungsverfahren für die Einspeisung aus Photovoltaik, Energiewirtschaftliche Tagesfragen

SKARTVEIT, A., J.A. OLSETH and M.E. TUFT, 1998, An hourly diffuse fraction model with correction for variability and surface albedo. SOLAR ENERGY, 63, 173-183, DOI: 10.1016/S0038-092X(98)00067-X

Thomaschki, K., Positionpapier zur verbesserten Prognose und Bilanzierung von Solarstromeinspeisung, Bundesnetzagentur, 2011